Statistics of ionospheric scintillation occurrence over European high latitudes

***V. Sreeja and M. Aquino**

Nottingham Geospatial Institute, University of Nottingham, Triumph Road, Nottingham NG7 2TU, United Kingdom

Abstract:

Rapid fluctuation in the amplitude and phase of transionospheric radio signals caused by small scale ionospheric plasma density irregularities is known as scintillation. Over the high latitudes, irregularities causing scintillation are associated with large scale plasma structures and scintillation occurrence is mainly enhanced during geomagnetic storms. This paper presents a statistical analysis of scintillation occurrence on GPS L1C/A signal at a high latitude station located in Bronnoysund (geographic latitude 65.5°N, geographic longitude 12.2°E; corrected geomagnetic (CGM) latitude 62.77°N), Norway, during the periods around the peaks of solar cycles 23 (2002-2003) and 24 (2011-2013). The analysis revealed that the scintillation occurrence at Bronnoysund during both the solar maximum periods maximises close to the midnight magnetic local time (MLT) sector. A higher occurrence of scintillation is observed on geomagnetically active days during both the solar maximum periods. The seasonal pattern of scintillation occurrence indicated peaks during the summer and equinoctial months. A comparison with the interplanetary magnetic field (IMF) components B_y and B_z showed an association of scintillation occurrence with the southward IMF B_z conditions.

Keywords: Auroral Ionosphere; Ionospheric Irregularities; Radio Wave Propagation

*Corresponding author: v.sreeja@gmail.com

1. Introduction:

Scintillation is characterised by rapid fluctuations in the amplitude and phase of transionospheric radio signals caused by small scale plasma density irregularities in the ionosphere [Kintner et al., 2001 and the references therein]. It is well known that scintillation can impair the tracking performance of Global Navigation Satellite System (GNSS) receivers [Aquino et al. 2005; Sreeja et al., 2012 and the references therein], thereby affecting the required levels of availability, accuracy and integrity, and consequently the reliability of modern day GNSS based applications. The occurrence of scintillation shows large day-to-day variability with dependence on local time, season, latitude, longitude as well as solar and geomagnetic activity. The global morphology of ionospheric L-band scintillation is presented in Basu et al. [2002], which reports that the scintillation occurrence is intense over the equatorial latitudes (extending from 20°N to 20°S geomagnetic latitudes), moderate at high latitudes (65° to 90° geomagnetic latitudes) and almost absent at the mid-latitudes. In the equatorial and high latitudes, the processes that govern the generation and sustenance of irregularities causing scintillation are quite different, thereby leading to significant differences in the observed characteristics of scintillation effects. One of the observed differences is a relatively higher occurrence of amplitude scintillation over the equatorial latitudes and, in contrast, a higher occurrence of phase scintillation over the high latitudes.

At high latitudes, irregularities causing scintillation are associated with large scale plasma structures and scintillation occurrence is mainly enhanced during geomagnetic storms, even in the solar minimum years [Aarons et al., 2000; Ngwira et al., 2010 and the references therein]. The plasma structuring is controlled by the magnetic coupling between the interplanetary magnetic field (IMF) and the magnetosphere [Hunsucker and Hargreaves, 2003]. The large scale plasma structures convect across the polar region and cause destabilisation of the plasma, leading to the generation of small scale irregularities causing scintillation [Valladares et al.

1994 and the references therein]. In the northern hemisphere, the irregularity oval is situated equatorward of the auroral oval and it expands equatorward with the increasing magnetic activity [Aarons and Allen, 1971].

Climatological studies have shown that over the northern and southern hemispheres, phase scintillation, as a function of magnetic local time (MLT) and geomagnetic latitude, is intense in the nightside auroral oval and on the dayside in the cusp region [Spogli et al., 2009; Li et al., 2010; Prikryl et al., 2011a]. Several studies have reported the observations of auroral and cusp scintillation and the influence of the IMF on the formation and dynamics of plasma patches during severe geomagnetic storms (like the Halloween storm of October 2003 or the geomagnetic storms of November 2004 or April 2010) [Mitchell et al., 2005; De Franceschi et al., 2008; Meggs et al., 2008; Prikryl et al., 2011b; Kinrade et al., 2012, and the references therein]. In a statistical study based on one year of data, Alfonsi et al. [2011] reported that in both the hemispheres, the IMF orientation influences mainly the scintillation distribution in MLT, thus highlighting the important role of the plasma inflow and outflow from and to the magnetosphere in the noon and midnight MLT hours. An analysis between the occurrence of scintillation and the southward IMF B_z conditions, along with the consequential impact on the tracking performance of a GNSS receiver located at a high-latitude station in Bronnoysund, Norway, was performed by Aquino and Sreeja [2013]. Their analysis revealed that the scintillation occurrence for selected geomagnetically disturbed days at this station was associated with the southward IMF B_z conditions.

In this context, this paper investigates statistically the occurrence of scintillation during the periods around the maximum phases of solar cycles 23 and 24 , at Bronnoysund (geographic latitude 65.5°N, geographic longitude 12.2°E; corrected geomagnetic (CGM) latitude 62.77°N), in Norway. The data and method of analysis used in this study are introduced in section 2. Section 3 presents the results and discussions,whereas the conclusions are presented in section 4.

2. Data and methodology:

The present study is based on the ionospheric scintillation data recorded on the GPS L1C/A signal at Bronnoysund around the maximum phase of solar cycle 23 (April 2002 to December 2003) by a NovAtel/AJ Systems GSV4004 [GPS Silicon Valley, 2004] receiver and around the maximum phase of solar cycle 24 (August 2011-June 2013) by a Septentrio PolaRxS [Septentrio PolaRxS, 2007] receiver. For each period, the data availability and with the averaged sunspot number (http://www.swpc.noaa.gov/ftpdir/weekly/RecentIndices.txt) are listed in Table 1. As this paper deals with a statistical representation, data from years 2002 and 2003 have been combined to represent the period around the maximum of solar cycle 23 (hereafter referred to as strong solar maximum), whereas data from years 2011, 2012 and 2013 have been combined to represent the period around the maximum of solar cycle 24 (hereafter referred to as weak solar maximum).

The PolaRxS and the GSV4004 receivers use similar algorithms to provide the amplitude scintillation index S_4 (standard deviation of the received signal power normalised by its mean value) and the phase scintillation index, SigmaPhi (standard deviation of the detrended carrier phase using a high pass filter with 0.1 Hz cutoff computed over 1, 3, 10, 30 and 60 seconds). Analyses presented in Sreeja et al. [2011] show that the scintillation indices recorded by the two receivers are comparable. In this study, the 60s SigmaPhi (Phi60) values are used. The S_4 is not considered since it was generally very low, even during periods of enhanced Phi60, as is usually the case at high latitudes [Kintner et al., 2007; Ngwira et al. 2010]. The percentage occurrence of Phi60 for 1 h MLT bin is calculated as:

$$100 * N(Phi60 > threshold)/N_{total} \qquad (1)$$

where *N (Phi60>threshold)* is the number of cases when Phi60>threshold and N_{total} is the total number of data points in the bin. As this study focuses on the occurrence of moderate to strong levels of scintillation, the threshold for Phi60 is chosen as 0.3 [Aquino et al. 2005 and the references therein]. The criterion defined as:

$$R = 100 \times \frac{\sigma(N_{total})}{N_{total}} > 0.025 \quad (2)$$

is chosen in order to remove the contribution of bins with poor statistics, where $\sigma(N_{total})$ is the standard deviation of the number of points in each bin [Taylor, 1997; Spogli et al., 2009; Prikryl et al., 2011a].

In this study, only measurements from satellites with an elevation angle greater than 15° are considered, in order to remove the contribution from non-scintillation related effects, such as multipath. This threshold on the satellite elevation angle implies that the CGM latitude range in the field of view from Bronnoysund at the sub-ionospheric height of 350 km is 54-72°N. Also, a lock time threshold of 240s is used to allow the convergence of the phase detrending filter.

The characterisation of the IMF components (B_y and B_z) is performed using the measurements made by the Magnetic Field Experiment (MAG) on board the Advanced Composition Explorer (ACE) satellite (http://www.srl.caltech.edu/ACE/). For this study, the hourly averaged IMF data is used. The planetary geomagnetic activity index, K_p, is obtained from the World Data Center for Geomagnetism, Kyoto (http://wdc.kugi. kyoto-u.ac.jp/).

3. Results and Discussions:

The percentage occurrence maps of Phi60>0.3 over Bronnoysund during the strong (left panel) and weak (right panel) solar maximum periods as a function of MLT and CGM latitude is shown in figure 1. The maps have a resolution of 1 hour in MLT and 1° in CGM latitude. The red lines represent the average equatorward and poleward positions of the statistical auroral oval for moderate geomagnetic activity level, IQ=3[Feldstein, 1963; Holzworth and Meng, 1975].

It can be observed from figure 1 that the percentage occurrence of scintillation, as expected, is higher during the strong solar maximum as compared to the weak solar maximum. The occurrence of scintillation maximises (>30%) close to the midnight, i.e. within the 23-02 h MLT sector and between 60-65°N CGM latitudes, during both the strong and weak solar maximum periods. The range of geomagnetic latitudes in the field of view from Bronnoysund at the sub-ionospheric height of 350 km and an elevation threshold of 15° falls on the edges of the IQ=3 auroral oval during the midnight MLT sector, thus explaining the high scintillation occurrence. Further, from figure 1 it is clear that the scintillation occurrence maximises near the CGM latitude of Bronnoysund (i.e. around 62.77°N), suggesting the field aligned nature of the irregularities. This is in agreement with what is presented in Kersley et al. [1988], where they have shown a similar feature in the occurrence of VHF scintillation at the European high latitude station of Kiruna (geographic latitude 67.83°N; geographic longitude 20.43°E; CGM latitude 64.3°N). It can also be observed that during the strong solar maximum, scintillation occurrence shows a secondary peak during the magnetic noon sector, i.e. 10-13 h MLT. This can be attributed to the fact that figure 1 encompasses data from varied geomagnetic conditions and that the auroral oval will expand with the increasing magnetic activity.

To study the association of scintillation occurrence with geomagnetic activity, the data from both the solar maximum periods has been separated into quiet and active sub-datasets, using the 3 hourly K_p index. A threshold of $K_p>3$ is chosen to represent geomagnetically active days. Figure 2 shows the scintillation occurrence as a function of MLT for the geomagnetically quiet (top panels) and active (bottom panels) days of both the strong (left panel) and weak (right panel) solar maximum periods.

From figure 2, it can be observed that, as expected, the scintillation occurrence during both the solar maximum periods is higher during the geomagnetically active days. This result is in agreement with what is presented in Aquino and Sreeja [2013], where they show a similar dependence of scintillation occurrence at Bronnoysund on K_p. Moreover, it is clear from the bottom panels of figure 2 that the scintillation occurrence observed during the magnetic local noon in figure 1 is associated with geomagnetically active conditions.

The seasonal pattern of scintillation occurrence as a function of MLT for the strong (left panel) and weak (right panel) solar maximum periods is shown in figure 3. The seasons have been separated assuming as summer the period May/June/July/August, as equinoxes the period March/April/September/October and as winter the period November/December/January/February.

From figure 3, a relatively higher occurrence of scintillation is observed in summer and equinoxes than in winter during both the solar maximum periods. This could be due to the fact that the electron density is generally lower in winter than in summer and equinoxes [Sojka et al., 1982]. It can be also observed from figure 3 that during summer and equinoxes, the occurrence of scintillation is largely in the 18-02 h MLT sector. The scintillation occurrence is observed in the magnetic local noon sector during winter of the strong solar maximum period. This indicates a seasonal pattern of scintillation occurrence in Bronnoysund which corroborates what is presented in Kersley et al. [1998], where a similar seasonal dependence for the VHF scintillation at Kiruna is shown.

It has been reported in Aquino and Sreeja [2013] that the scintillation occurrence at Bronnoysund is largely controlled by the IMF conditions. To investigate this aspect further, the association of scintillation occurrence with the polarity of the IMF components B_y and B_z during the strong (left panel) and weak (right panel) solar maximum periods is shown in figures 4a and 4b respectively. These figures show the scintillation occurrence as a function of MLT.

In comparing the IMF B_z northward ($B_z>0$) and southward ($B_z\leq0$) conditions in the bottom panels of figures 4a and 4b, it can be observed that in general for B_z southward conditions, scintillation occurrence peaks in the 18-02 h MLT sector and that the associated scintillation occurrence percentage is higher. It can also be observed that for southward B_z conditions, scintillation occurs in the magnetic local noon sector during the strong solar maximum period. The IMF components are measured at the L1 Lagragian point and therefore the IMF components have to be shifted to account for the convection time delay from the L1 point to magnetosphere. However, as this study deals with a statistical representation, the IMF components have not been shifted and this could be the possible reason for the relatively smaller percentage of scintillation occurrence observed during northward IMF B_z conditions. Considering the association of scintillation occurrence with IMF B_y**,** the top panels of figures 4a and 4b show that there is no significant difference in the scintillation occurrence pattern for positive and negative values of IMF B_y. The analysis of figures 4a and 4b confirms that scintillation occurrence at Bronnoysund is strongly associated with southward IMF B_z condition$_s$. This could possibly be linked to the occurrence of polar cap patches during southward IMF B_z [Valladares et al. 1994 and the references therein].

4. Conclusions:

A statistical analysis of the scintillation occurrence on the GPS L1C/A signal around the maximum of solar cycles 23 (2002-2003) and 24 (2011-2013) at a high latitude station in Bronnoysund (geographic latitude 65.5°N, geographic longitude 12.2°E; CGM latitude 62.77°N), Norway, is presented. Analyses revealed that the scintillation occurrence follows the auroral oval and maximises close to the midnight MLT sector (23-02 h). The scintillation occurrence at this station is strongly controlled by the geomagnetic conditions, with a higher occurrence during the geomagnetically active days. Also, the scintillation occurrence has a seasonal pattern, with peaks during summer and equinoctial months. A comparison with the IMF components B_y and B_z showed a strong association of scintillation occurrence with southward IMF B_z conditions.

Acknowledgements:

Research activities related to this paper at the Nottingham Geospatial Institute, University of Nottingham are funded by the UK Engineering and Physical Sciences Research Council project, Polaris (grant number: EP/H003479/1, http://www.bath.ac.uk/elec-eng/polaris/). Authors would like to thank the ACE MAG instrument team and the ACE Science Center for providing the ACE data,,the Space Weather Prediction Center for providing the solar data and the World Data Center (WDC) for Geomagnetism, Kyoto for providing the geomagnetic data.

References:

Aarons, J., Lin, B., Mendillo, M., Liou, K., Codrescu, M., 2000, Global Positioning System phase 4uctuations and ultraviolet images from the Polar satellite, J. Geophys. Res., 105, 5201-5213.

Aarons, J., Allen, R., 1971, Scintillation Boundary during Quiet and Disturbed Magnetic Conditions, J. Geophys. Res., 76, 170-177.

Alfonsi, L., Spogli, L., De Franceschi, G., Romano, V., Aquino, M., Dodson, A., Mitchell, C. N., 2011, Bipolar climatology of GPS ionospheric scintillation at solar minimum, Radio Sci., 46, RS0D05, doi:10.1029/2010RS004571.

Aquino, M., Rodrigues, F. S., Souter, J., Moore, T., Dodson, A., Waugh, S., 2005, Ionospheric scintillation and impact on GNSS users in Northern Europe: Results of a 3 Year Study, Space Communications - Propagation Modelling for Space Radio Frequency, 20, 17-29, IOS Press Amsterdam, The Netherlands.

Aquino, M., Sreeja, V., 2013, Correlation of scintillation occurrence with interplanetary magnetic field reversals and impact on Global Navigation Satellite System receiver tracking performance, Space Weather, 11, doi:10.1002/swe.20047.

Basu, S., Groves, K. M., Basu, Su., Sultan, P. J., 2002, Specification and forecasting of scintillations in communication/navigation links: current status and future plans, J. Atmos. Solar-Terr. Phys., 64, 1745–1754.

De Franceschi, G., Alfonsi, L., Romano, V., Aquino, M., Dodson, A., Mitchell, C. N., Spencer, P., Wernik, A. W., 2008, Dynamics of high latitude patches and associated small scale irregularities during the October and November 2003 storms, J. Atmos. Solar-Terr. Phys., 70, 879-888.

Feldstein, Y. I. (1963), On Morphology and Auroral and Magnetic Disturbances at High Latitudes, Geomagn. Aeron., 3, 183–192.

GPS Silicon Valley (2004), GSV4004/GSV4004A GPS Ionospheric Scintillation & TEC Monitor (GISTM) user’s manual.

Hunsucker, R. D., Hargreaves, J. K., 2003, The high-latitude F region and the trough, in The High-Latitude Ionosphere and Its Effects on Radio Propagation, 227–281, Cambridge Univ. Press, Cambridge, U. K.

Holzworth, R. H., Meng, C., -I.,1975, Mathematical Representation of the Auroral Oval, Geophys. Res. Lett., 2, 377–380.

Kersley, L., Pryse, S. E., Wheadon, N. S., 1988, Amplitude and phase scintillation at high latitudes over northern Europe, Radio Sci., 23, 320-330.

Kinrade, J., Mitchell, C. N., Yin, P., Smith, N., Jarvis, M. J., Maxfield, D. J., Rose, M. C., Bust, G. S., Weatherwax, A. T., 2012, Ionospheric scintillation over Antarctica during the storm of 5–6 April 2010, J. Geophys. Res., 117, A05304, doi:10.1029/2011JA017073.

Kintner P. M., Kil, H., Beach, T. L., de Paula, E. R., 2001, Fading Timescales Associated with GPS Signals and Potential Consequences, Radio Sci., 36, 731-743, doi:10.1029/1999RS002310.

Kintner, P. M., Ledvina, B. M., de Paula, E. R., 2007, GPS and ionospheric scintillations, Space Weather, 5, S09003, doi:10.1029/2006SW000260.

Li, G., Ning, B., Ren, Z., Hu, L., 2010, Statistics of GPS ionospheric scintillation and irregularities over polar regions at solar minimum GPS Solutions, 14, doi:10.1007/s10291-009-0156-x.

Meggs, R.W., Mitchell, C. N., Honary, F., 2008, GPS Scintillation over the European Arctic during the November 2004 storms, GPS Solut, 12, 281–287, doi:10.1007/s10291-008-0090-3.

Mitchell, C. N., Alfonsi, L., De Franceschi, G., Lester, M., Romano, V., Wernik, A. W., 2005, GPS TEC and scintillation measurements from the polar ionosphere during the October 2003 storm, Geophys Res Lett, 32, L12S03, doi:10.1029/2004GL021644.

Ngwira C. M., McKinnell L. A., Cilliers P. J., 2010, GPS phase scintillation observed over a high-latitude Antarctic station during solar minimum, J. Atmos. Solar-Terr. Phys., 72, 718-725.

Prikryl, P., Jayachandran, P. T., Mushini, S. C., Chadwick, R., 2011a, Climatology of GPS phase scintillation and HF radar backscatter for the high-latitude ionosphere under solar minimum conditions, Ann. Geophys., 29, 377-392, doi:10.5194/angeo-29-377-2011.

Prikryl, P., Spogli, L., Jayachandran, P. T., Kinrade, J. et al., 2011b, Interhemispheric comparison of GPS phase scintillation at high latitudes during the magnetic-cloud-induced geomagnetic storm of 5–7 April 2010, Ann. Geophys., 29, 2287–2304, doi:10.5194/angeo-29-2287-2011.

Septentrio PolaRxS (2007), Septentrio PolaRxS RxControl version 3.1 user manual.

Spogli, L., Alfonsi, L., De Franceschi, G., Romano, V., Aquino, M., Dodson, A., 2009, Climatology of GPS ionospheric scintillations over high and mid-latitude European regions, Ann. Geophys., 27, 3429-3437.

Sreeja, V., Aquino, M., Elmas, Z. G., Forte, B., 2012, Correlation analysis between ionospheric scintillation levels and receiver tracking performance, Space Weather, 10, S06005, doi:10.1029/2012SW000769.

Sreeja, V., Aquino, M., Forte, B. et al., 2011, Tackling Ionospheric Scintillation Threat to GNSS in Latin America, Journal of Space Weather and Space Climate, 1, A05, doi:10.1051/swsc/2011005.

Taylor, J. R., 1997, An introduction to Error Analysis: The Study of Uncertainties in Physical Measurement, 2nd ed., University Science Books, USA.

Valladares, C. E., Basu, S., Buchau, J., Friis-Christiansen, E., 1994, Experimental Evidences for the Formation and Entry of Patches into the Polar Cap, Radio Sci., 29, 167-194.

Table captions:

Table 1: Data availability over Bronnoysund along with the averaged sunspot number

Figure captions:

Figure 1: Percentage occurrence of Phi60>0.3 as a function of MLT and CGM latitude during the solar maximum (left panel) and minimum (right panel) period. Red lines show the average equatorward and poleward positions of the Feldstein statistical auroral oval for moderate geomagnetic conditions, IQ=3.

Figure 2: Percentage occurrence of Phi60>0.3 as a function of MLT for geomagnetically quiet (top panels) and active (bottom panels) days during the strong (left panel) and weak (right panel) solar maximum periods.

Figure 3: Percentage occurrence of Phi60>0.3 as a function of MLT for the different seasons during the strong (left panel) and weak (right panel) solar maximum periods.

Figure 4a: Percentage occurrence of Phi60>0.3 rad as a function of MLT for observations made at Bronnoysund during strong solar maximum.

Figure 4b: Percentage occurrence of Phi60>0.3 as a function of MLT for observations made at Bronnoysund during weak solar maximum.

Table 1: Data availability over Bronnoysund along with the averaged sunspot number

Year	Days of data	Averaged sunspot number
2002	251	177
2003	340	109
2011	142	80
2012	288	82
2013	148	94

Figure 1

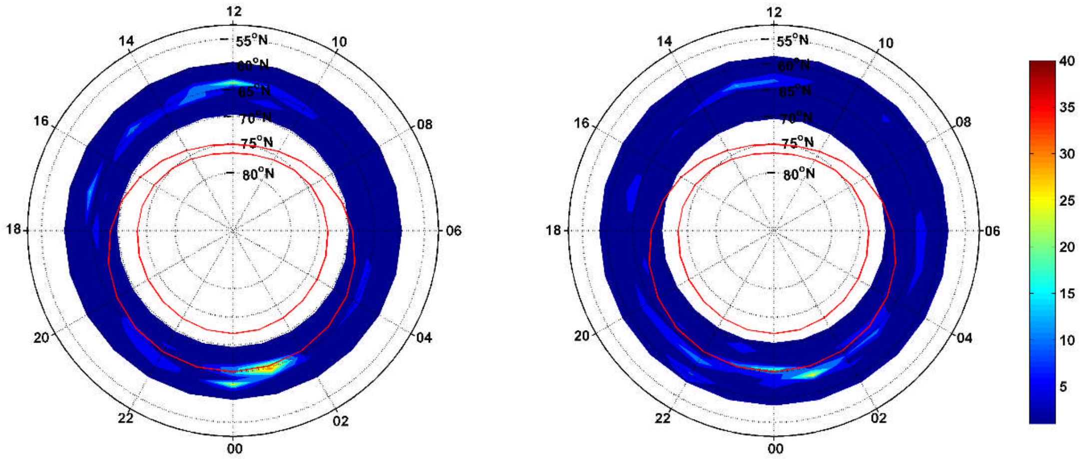
12
14
10
16
08
18
06
20
04
22
02
00
55°N
60°N
65°N
70°N
75°N
80°N
40
35
30
25
20
15
10
5

Figure 2

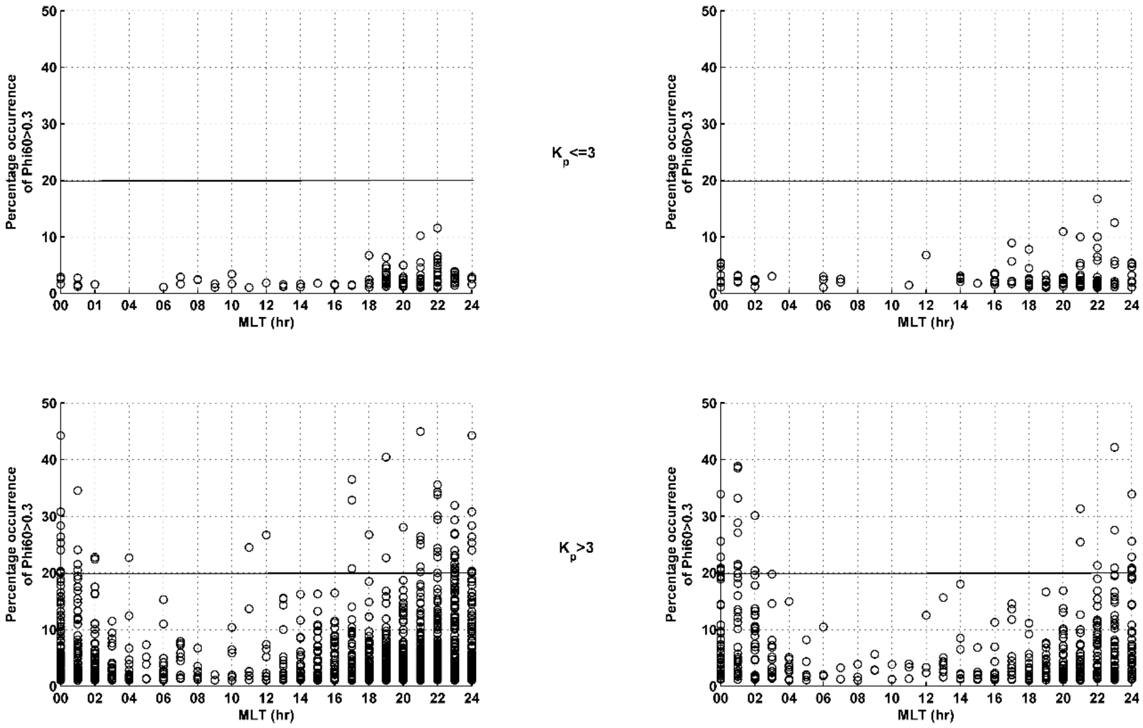

Figure 3

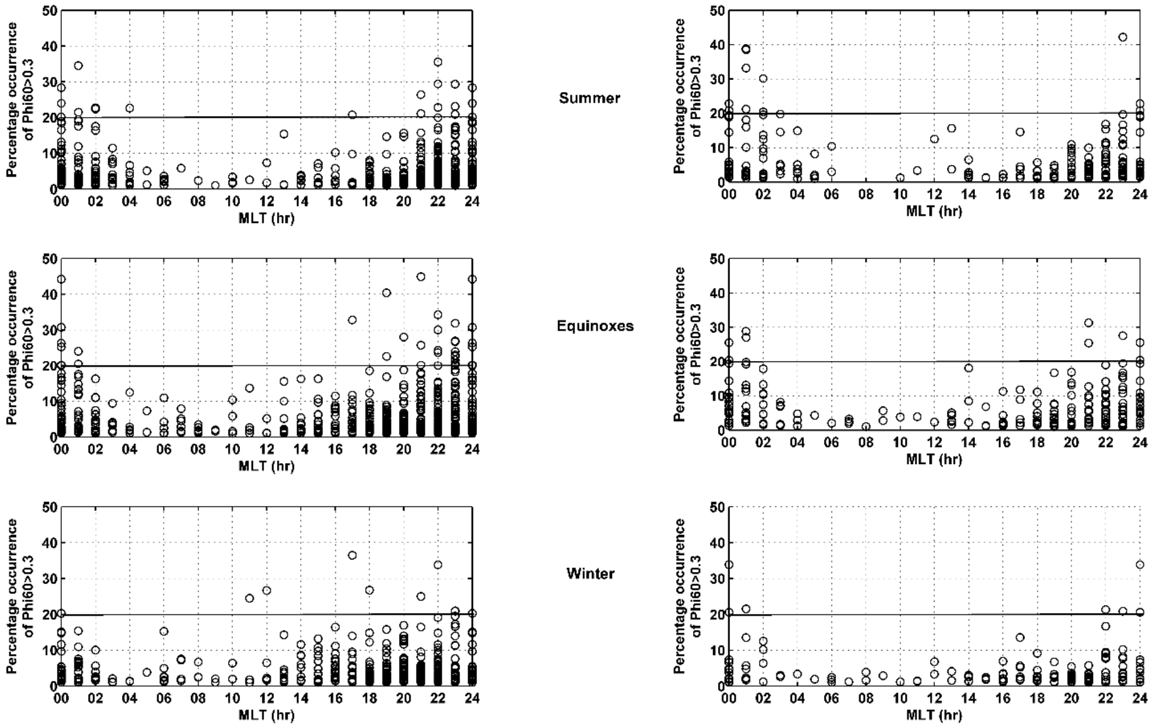
Summer
Equinoxes
Winter
Percentage occurrence of Phi60>0.3
MLT (hr)

Figure 4a

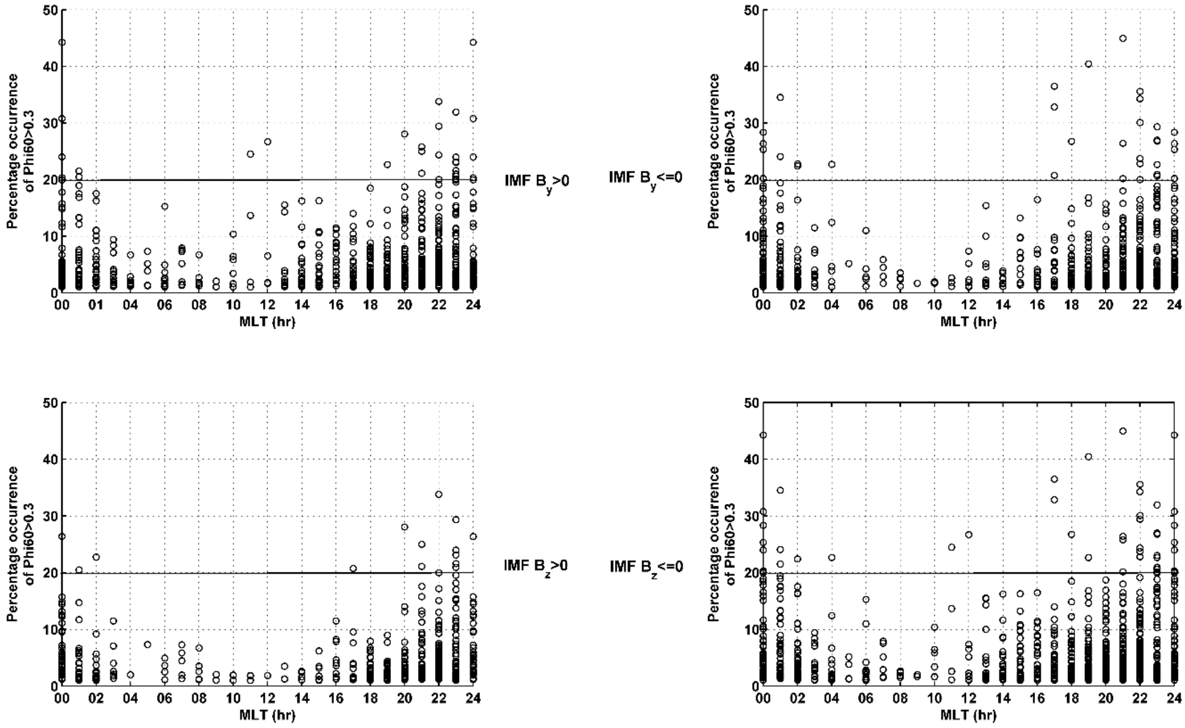
Percentage occurrence of Phi60>0.3
MLT (hr)
IMF B_y>0
IMF B_y<=0
IMF B_z>0
IMF B_z<=0

Figure 4b

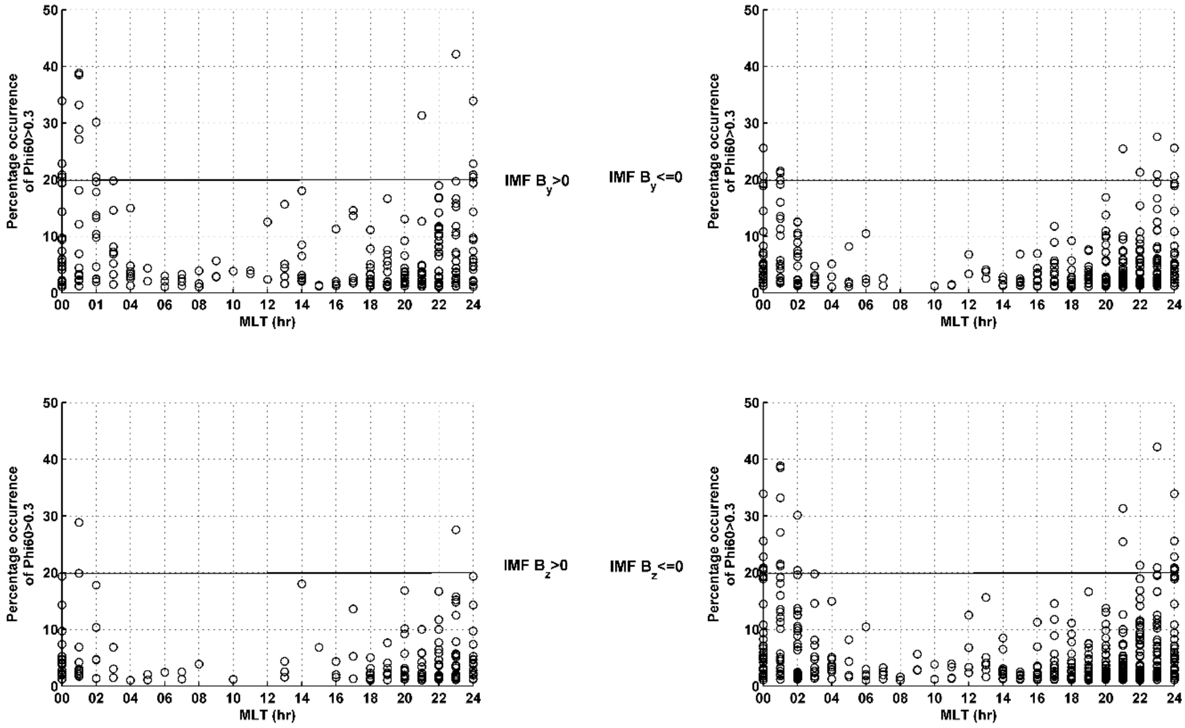
Percentage occurrence of Phi60>0.3
MLT (hr)
IMF B_y>0
IMF B_y<=0
IMF B_z>0
IMF B_z<=0